

Numerical Heat Transfer, Part B: Fundamentals

An International Journal of Computation and Methodology

ISSN: (Print) (Online) Journal homepage: www.tandfonline.com/journals/unhb20

Frictional heating effects on entropy generation with nonlinear Rosseland radiation: Implementation of generalized differential quadrature method

Muhammad Idrees Afridi, Yimiao Zhang, Ali J. Chamkha & Muhammad Samad Khan

To cite this article: Muhammad Idrees Afridi, Yimiao Zhang, Ali J. Chamkha & Muhammad Samad Khan (20 Apr 2024): Frictional heating effects on entropy generation with nonlinear Rosseland radiation: Implementation of generalized differential quadrature method, Numerical Heat Transfer, Part B: Fundamentals, DOI: [10.1080/10407790.2024.2343330](https://doi.org/10.1080/10407790.2024.2343330)

To link to this article: <https://doi.org/10.1080/10407790.2024.2343330>



Published online: 20 Apr 2024.



Submit your article to this journal [↗](#)





View related articles [↗](#)



View Crossmark data [↗](#)



Frictional heating effects on entropy generation with nonlinear Rosseland radiation: Implementation of generalized differential quadrature method

Muhammad Idrees Afridi^a , Yimiao Zhang^a, Ali J. Chamkha^b , and Muhammad Samad Khan^c

^aSchool of Mathematics and Computer Science, Hanjiang Normal University, Shiyan, P.R. China; ^bFaculty of Engineering, Kuwait College of Science and Technology, Kuwait City, Kuwait; ^cDepartment of Mathematics, NED University of Engineering and Technology, Karachi, Pakistan

ABSTRACT

This article examines heat transfer and entropy generation analysis for boundary layer flow, considering the impacts of frictional heating and nonlinear Rosseland thermal radiation. The equations governing momentum and energy in a two-dimensional boundary layer are transformed into self-similar equations *via* similarity operations. The generalized differential quadrature method (GDQM) is then used to numerically solve the non-dimensional governing equations. Entropy generation and Bejan numbers are computed using the acquired solutions and are then plotted against the emerging flow parameters. An in-depth analysis of temperature distribution, entropy generation, velocity profile, and Bejan number. A high level of agreement was seen when the results from the literature were replicated using GDQM to verify the accuracy of the numerical code. It is found that a self-similar solution exists in the presence of viscous dissipation. The primary contributor to entropy generation at the interface is fluid friction, in contrast to heat transfer. Further, the findings indicate that entropy generation positively correlates with the Prandtl number, heating parameter, radiation parameter, and Eckert number. Notably, the results show that a decrease in operational temperature causes a decrease in entropy production.

ARTICLE HISTORY

Received 13 November 2023
Revised 4 April 2024
Accepted 9 April 2024

KEYWORDS

Bejan number; entropy generation minimization; frictional heating; GDQM; Rosseland nonlinear thermal radiation

1. Introduction

Any object with a temperature greater than absolute zero will release electromagnetic waves as a form of energy. In high-temperature environments, including cooling systems, solar power technologies, hypersonic flights, and rocket combustion chambers, thermal radiation has a considerable impact on the consequences of heat transfer. The initial investigation on the influence of thermal radiation on boundary layer flow was carried out by Smith [1]. He found that the presence of gas radiation in the boundary layer can result in elevated temperatures on the wedge, which in turn impacts the recovery factors downstream in flat-plate wind-tunnel models that have laminar boundary layers.

When accounting for both convection and thermal radiation, the process of solving the energy conservation equation becomes mathematically complex. To simplify this complexity, the Rosseland approximation is employed. The effects of thermal radiation within the boundary layer

Nomenclature

| | | | |
|-------------------------|------------------------------------|--|--|
| a_R | Rosseland absorption coefficient. | $\{u, v\}$ u_w | Velocity components Velocity of moving boundary |
| Be | Bejan number | (x, y) | Cartesian coordinates |
| c_p | Specific heat at constant pressure | | |
| C_f | Skin friction coefficient | | |
| e_b | Black body emissive power | ρ | Density |
| Ec | Ecker number | σ_{SB} | Stefan-Boltzmann constant |
| $\{f(\eta), f'(\eta)\}$ | Unitless velocity functions | θ | Unitless temperature |
| k | Thermal Conductivity | θ_r | Heating Parameter |
| N_R | Radiation parameter | μ | Dynamic viscosity, |
| $Ns(\eta)$ | Unitless entropy generation | η | Unitless coordinate along the y-axis |
| Nu_x | Nusselt's Number | ν | Kinematic viscosity |
| Pr | Prandtl number | $\Theta(\eta)$ | Temperature function, [-] |
| q_r | Radiative heat flux | $\{\Theta'(\eta), \Theta''(\eta)\}$ | Derivatives of the function $\Theta(\eta)$ w.r.t. η , [-] |
| \dot{S}_{gen}''' | Entropy generation | ρ | Nanofluid density, [$kg.m^{-3}$] |
| $(\dot{S}''')_0$ | Characteristic entropy generation | | |
| T | Temperature | | |
| T_w | Temperature at boundary | | |
| T_∞ | Free-stream temperature | | |
| | | Operator | |
| | | $\nabla \langle = \frac{\partial}{\partial x} \hat{i} + \frac{\partial}{\partial y} \hat{j} + \frac{\partial}{\partial z} \hat{k} \rangle$ | Del operator |

have been investigated by researchers, as demonstrated by the work of Perdakis and Raptis [2]. This work examines the flow of a micropolar fluid past a stationary plate in a steady state, taking into account the influence of radiation. A numerical solution for the temperature distribution has been obtained and the impact of the radiation parameter on the temperature field is addressed.

Researchers applied the linearized Rosseland approximation, which is dependable only when there is a limited temperature differential between the solid border and the surrounding fluid [3–7]. In contrast to the previously accepted two-parameter approach, Magyari and Pantokratoras [8] presented evidence indicating that a single-parameter solution is adequate for addressing the linear Rosseland approximation problem. Pantokratoras and Fang [9–10] investigated the effects of nonlinear Rosseland thermal radiation on conventional Blasius and Sakiadis flows. The research findings show that the nonlinear Rosseland radiation approximation is correct for a wide range of temperature differences between the wall and the bulk fluid, including both low and high values. The temperature profile in the nonlinear Rosseland approximation differs from the linear approximation, exhibiting an S-shaped curve.

Numerous scientific, commercial, and technical applications exist for the study of boundary layer flow across a solid boundary. These applications include glass fiber production, wire drawing, and crystal growth. They also include operations such as extruding a polymer sheet from a die and producing materials *via* extrusion methods. To optimize the manufacturing process and guarantee the caliber and uniformity of the finished product, it is essential to comprehend the dynamics of boundary layer flow over a solid surface. Sakiadis [11] initially investigated the flow of a boundary layer that is propelled by a rigid flat surface. This study formulates fundamental differential and integral momentum equations for boundary-layer motion over unbroken solid boundaries, with a specific emphasis on two-dimensional and axisymmetric motion, introducing a novel category of boundary-layer challenges. Tsou et al. [12] subsequently conducted experiments on the aforementioned problem in controlled laboratory settings and observed a strong correlation with theoretical findings. Based on the findings from the laminar experiments and the strong correspondence observed between the measured profiles and theoretical predictions, they concluded that a mathematically describable boundary layer on a continuously moving surface

represents a feasible flow phenomenon. Subsequently, numerous scholars conducted studies on the Sakiadis flow while altering different physical parameters. In a study conducted by Cortell [13], the impact of linear Rosseland thermal radiation on Sakiadis flow was examined. The findings indicated that in fluids with lower values of Pr number, the surface temperature was observed to be high, and the surface temperature was low when N_R is large. In their research, Takhar et al. [14] investigated the flow of the boundary layer over a flat plate that is continuously moving. The study also considered the impact of variable fluid properties. The findings of the study revealed a positive correlation between the heating parameter $\frac{T_w}{T_\infty}$ and the velocity and temperature profile of the flow. The impact of suction and injection on the flow over a flat plate with constant velocity was examined by Fox et al. [15]. They concluded that the Von Karman-Pohlhausen technique, adapted to incorporate suction and injection effects, holds a broad scope of validity. This approach yields satisfactory results for the transfer coefficients associated with heat, mass, and momentum exchange across a wide range of parameters. The study conducted by Afzal et al. [16] involved an analysis of the characteristics of momentum and heat transfer in the context of fluid flow over a flat surface that is continuously moving in a parallel stream. Ishak [17] extended the examination conducted by Afzal et al. [16] to incorporate the impacts of linear thermal radiation. In this study, they reported that the radiation hinders the heat transfer process on a moving plate within a parallel flow, resulting in the emergence of two solutions in cases where the plate and fluid exhibit opposite movements. The Sakiadis flow of nanofluids with Newtonian heating in the presence of viscous dissipation was investigated by Makinde [18]. It reveals a rise in heat transfer as the nanoparticle volume fraction and Newtonian heating increase, while a decrease is observed with the Brinkmann number. The study conducted by Pantokratoras [19] focused on analyzing the effects of Blasius and Sakiadis flow on a Riga plate. The study assumed that the fluid properties were dependent on temperature.

The examination of fluid flows and their second law, specifically the generation of entropy, holds significant importance in the discipline of engineering systems. Prior research has investigated this subject matter in diverse physical flow scenarios [20–26]. However, there is a lack of comprehensive research on the analysis of entropy generation in boundary layer flows [27–31]. The primary aim of this scientific paper is to investigate the phenomenon of entropy production in the Sakiadis flow by considering the nonlinear Rosseland thermal radiation with viscous heating. Through the utilization of suitable similarity transformations, the fundamental governing equations undergo a conversion process, resulting in the production of a system of nonlinear ordinary differential equations. By means of these modifications, a dimensionless equation for the rate of entropy generation per unit volume is produced. To obtain numerical results, the Generalized Differential Quadrature Method (GDQM) is used. The model description and steps of differential quadrature scheme is shown in Figure 1.

2. Problem formulation

Let us consider the laminar, two-dimensional, steady, and incompressible boundary layer flow of a Newtonian fluid over a thin, rigid, and flat plate. The plate is impermeable and presumed to move at a constant velocity u_w . The coordinate system is established by situating its origin at the foremost edge of the plate, where the x – axis is aligned in parallel with the plate, while the y – axis is oriented perpendicular to it as shown in Figure 2. It is further assumed that the plate's temperature (T_w) remains unchanged. The derivation of the mass, momentum, and energy conservation equations is conducted by employing the Prandtl boundary layer approximation as [21]

$$\frac{\partial u}{\partial x} + \frac{\partial v}{\partial y} = 0 \quad (1)$$

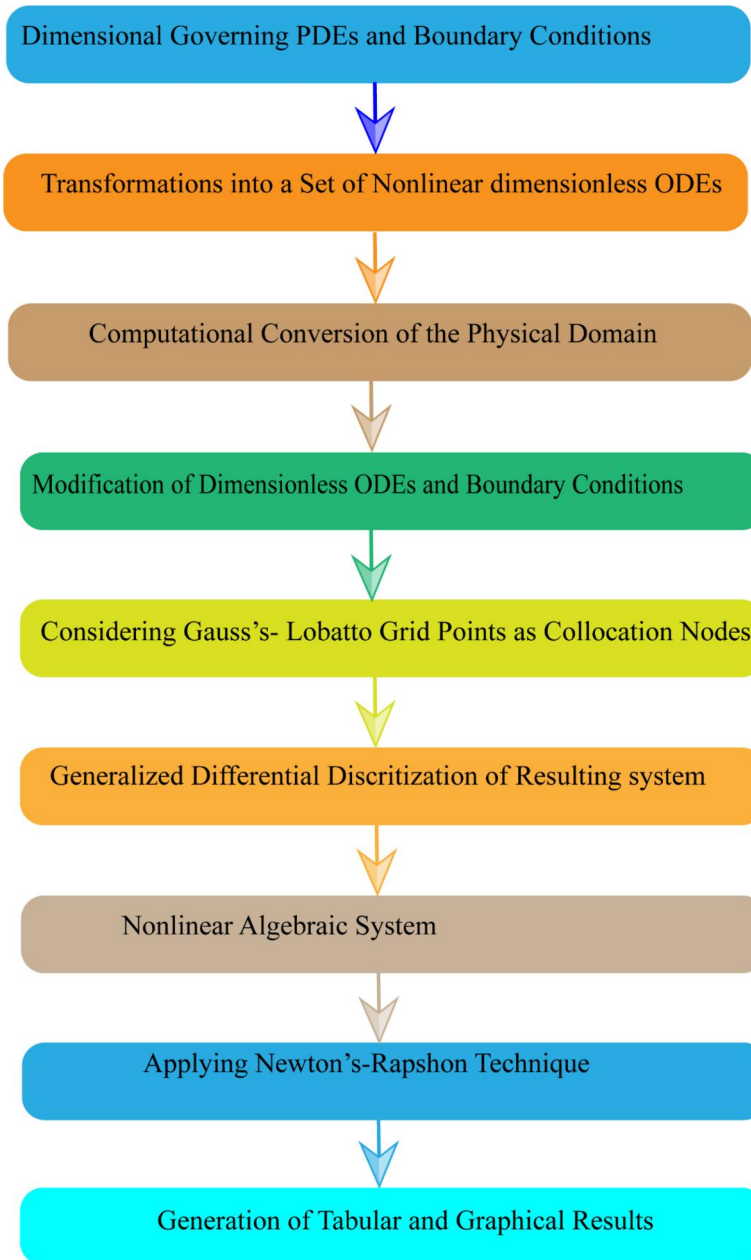


Figure 1. Flowchart for the system description and applied numerical algorithm.

$$u \frac{\partial u}{\partial x} + v \frac{\partial u}{\partial y} = \nu \frac{\partial^2 u}{\partial y^2} \quad (2)$$

$$u \frac{\partial T}{\partial x} + v \frac{\partial T}{\partial y} = \frac{1}{\rho c_p} \left(k \frac{\partial^2 T}{\partial y^2} + \mu \left(\frac{\partial u}{\partial y} \right)^2 - \frac{\partial q_r}{\partial y} \right) \quad (3)$$

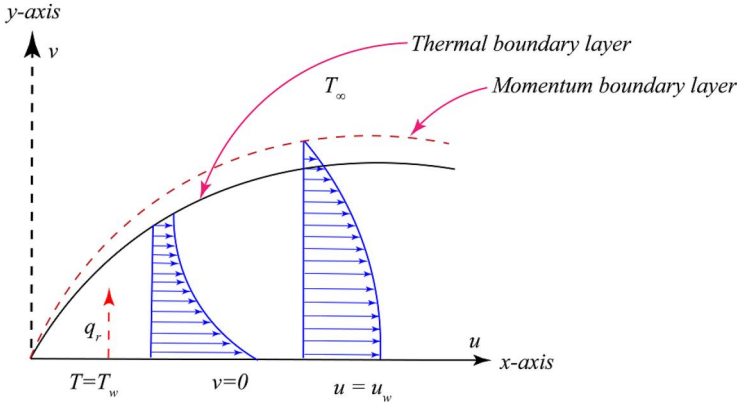


Figure 2. Geometry of the flow configuration.

The relative Boundary conditions are [9]

$$\left. \begin{aligned} u(x, y = 0) &= u_w \\ v(x, y = 0) &= 0 \\ T(x, y = 0) &= T_w \end{aligned} \right\}. \quad (4)$$

$$\left. \begin{aligned} u(x, y \rightarrow \infty) &\rightarrow 0 \\ T(x, y \rightarrow \infty) &\rightarrow T_\infty \end{aligned} \right\}. \quad (5)$$

In the provided context, the variables u and v are used to denote the components of velocity in the x and y directions, respectively. The symbol " T_∞ " is used to represent the temperature of the fluid outside the boundary layer. The symbol " ν " represents the kinematic viscosity of the fluid. The symbol " k " indicates the thermal conductivity of the fluid. The symbol " μ " represents the dynamic viscosity of the fluid. The symbol " c_p " denotes the specific heat at constant pressure. The symbol " q_r " represents the radiative heat flux. Lastly, the symbol " ρ " represents the density of the fluid. The expression for the radiative heat flux in the case of optically thick materials can be expressed using the Rosseland approximation as follows [1]

$$q_r = -\frac{4}{3a_R} \nabla(e_b), \quad (6)$$

where $\nabla \equiv \hat{i} \frac{\partial}{\partial x} + \hat{j} \frac{\partial}{\partial y} + \hat{k} \frac{\partial}{\partial z}$ is vector differential operator, $e_b(Wm^{-2})$ and $a_R(1/m)$ respectively indicate black body emissive power and Rosseland absorption coefficient. Using the Stefan-Boltzmann law ($e_b = \sigma_{SB} T^4$, σ_{SB} is Stefan-Boltzmann constant), Equation (6) takes the following form

$$q_r = -\frac{16\sigma_{SB}}{3a_R} T^3 \frac{\partial T}{\partial y}. \quad (7)$$

Upon substitution of Equation (7) into Equation (3), we get

$$u \frac{\partial T}{\partial x} + v \frac{\partial T}{\partial y} = \frac{1}{\rho c_p} \left(k \frac{\partial^2 T}{\partial y^2} + \frac{4\sigma_{SB}}{3a_R} \frac{\partial^2 (T^4)}{\partial y^2} + \mu \left(\frac{\partial u}{\partial y} \right)^2 \right). \quad (8)$$

The subsequent similarity transformations are employed to derive similarity equations.

$$\eta = y \sqrt{\frac{u_w}{x\nu}}, \quad u = u_w f'(\eta), \quad v = \frac{1}{2} \sqrt{\frac{u_w \nu}{x}} (\eta f' - f), \quad \theta(\eta) = \frac{T - T_\infty}{T_w - T_\infty}. \quad (9)$$

Using Equation (9), the self-similar form of Equations (2 and 3) is

$$f''' + \frac{1}{2}ff'' = 0 \quad (10)$$

$$N_R\theta'' + EcPrN_Rf''^2 + \frac{1}{2}PrN_R\theta'f + \frac{1}{3}\frac{[(\theta(\theta_r - 1) + 1)^4]''}{\theta_r - 1} = 0. \quad (11)$$

The boundary conditions are

$$f(0) = 0, \quad f'(0) = 1, \quad f'(\infty) = 0, \quad (12)$$

$$\theta(0) = 1, \quad \theta(\infty) = 0, \quad (13)$$

where

$$\left\{ \begin{array}{l} Ec = \frac{u_w^2}{c_p (T_w - T_\infty)} \text{ (Eckert number),} \\ N_R = \frac{a_R k}{4\sigma_{SB} T_\infty^3} \text{ (Radiation parameter),} \\ Pr = \frac{\nu}{\alpha} \text{ (Prandtl number),} \\ \theta_r = \frac{T_w}{T_\infty} \text{ (Heating parameter).} \end{array} \right.$$

The local skin friction coefficient and the local Nusselt number are the two main physical characteristics of importance. Fundamentally, the skin friction coefficient represents the dimensionless shear stress at the wall, while the Nusselt number represents the rate of heat transfer at the wall. According to a precise definition, the local skin friction coefficient is

$$C_f = \frac{2\tau_w(x)}{\rho(u_w)^2}, \quad (14)$$

here

$$\tau_w = \mu \left(\frac{\partial u}{\partial y} \right)_{y=0} \quad (15)$$

The local Nusselt number is given by

$$Nu_x = \frac{q_w x}{k(T_w - T_\infty)}, \quad (16)$$

here

$$q_w = -k \left(\frac{\partial T}{\partial y} \right)_{y=0} + (q_r)_{y=0} = - \left(k + \frac{16\sigma_{SB}}{3a_R} T_w^3 \right) \left(\frac{\partial T}{\partial y} \right)_{y=0}. \quad (17)$$

The Nusselt number and skin friction coefficient can be written as follows after applying the changes mentioned in Equation (9).

$$\left\{ \begin{array}{l} \frac{1}{2} C_{fx} (\text{Re}_x)^{1/2} = f''(0) \\ \frac{Nu_x}{(\text{Re}_x)^{1/2}} = -\theta'(0) \left(1 + \frac{4}{3N_R} (\theta_r)^3 \right). \end{array} \right. \quad (18)$$

3. Entropy generation

The Prandtl boundary layer assumptions and the second law of thermodynamics can be utilized to express the entropy production that features frictional dissipation and nonlinear Rosseland thermal radiation as [21]

$$\dot{S}'''_{gen} = \frac{k}{T^2} \left(\frac{\partial T}{\partial y} \right)^2 \left(1 + \frac{16\sigma_{SB}T^3}{3a_Rk} \right) + \frac{\mu}{T} \left(\frac{\partial u}{\partial y} \right)^2. \quad (19)$$

Equation (19) illustrates that in the presence of gradients in velocity or temperature, the entropy production rate is both positive and finite. Equation (19) illustrates the existence of two distinct sources of entropy generation, represented by the two terms located on the right-hand side. The initial term denotes the thermal energy transfer irreversibility, whereas the subsequent expression signifies the generation of entropy caused by fluid friction.

3.1. Entropy generation number

Through the utilization of dimensionless variables, Equation (19) can be reformulated in relation to the entropy generation number $Ns(\eta)$, which represents the volumetric rate of entropy production in a dimensionless form.

$$Ns(\eta) = \frac{\dot{S}'''_{gen}}{\left(\dot{S}'''_{gen} \right)_o} = \frac{(\theta_r - 1)^2 \theta'^2}{(\theta(\theta_r - 1) + 1)^2} + \frac{Ec \ Pr \ f''^2(\theta_r - 1)}{\theta(\theta_r - 1) + 1} + \frac{4(\theta(\theta_r - 1) + 1)\theta'^2(\theta_r - 1)^2}{3N_R}, \quad (20)$$

here

$$\begin{cases} N_H = \frac{(\theta_r - 1)^2 \theta'^2}{(\theta(\theta_r - 1) + 1)^2} + \frac{4(\theta(\theta_r - 1) + 1)\theta'^2(\theta_r - 1)^2}{3N_R}, \\ N_F = \frac{Ec \ Pr \ f''^2(\theta_r - 1)}{\theta(\theta_r - 1) + 1}, \\ \left(\dot{S}'''_{gen} \right)_o = \frac{kU}{\nu x}. \end{cases} \quad (21)$$

3.2. Bejan number

Although the entropy generation number Ns offers insights into the spatial distribution of the entropy generation profile, it may not be adequate for addressing energy optimization issues. Such problems necessitate a comprehensive comprehension of the proportional contributions of the thermal component and fluid friction to the overall entropy production. The Bejan number is defined as a measure for quantifying the dominance of two sources and defined as follow:

$$Be = \frac{\frac{k}{T^2} \left(\frac{\partial T}{\partial y} \right)^2 \left(1 + \frac{16\sigma_{SB}T^3}{3a_Rk} \right)}{\frac{\mu}{T} \left(\frac{\partial u}{\partial y} \right)^2 + \frac{k}{T^2} \left(\frac{\partial T}{\partial y} \right)^2 \left(1 + \frac{16\sigma_{SB}T^3}{3a_Rk} \right)}. \quad (22)$$

Using Equation (9), the reduced form of Equation (22) is

$$Be(\eta) = \frac{(3N_R + 4(\theta(\theta_r - 1) + 1)^3)\theta'^2(\theta_r - 1)}{3N_R(\theta_r - 1)\theta'^2 + 3N_R Ec Pr f''^2(\theta(\theta_r - 1) + 1) + 4(\theta_r - 1)(\theta(\theta_r - 1) + 1)^3\theta'^2}. \quad (23)$$

When $Be < 0.5$, the impact of fluid friction on entropy generation surpasses that of heat transfer. In contrast, when $Be > 0.5$ the impact of heat transfer on the production of entropy surpasses that of fluid friction. When $Be = 0.5$ the generation of entropy is equally influenced by both fluid friction and heat transfer.

4. Solution methodology

The computational domain is $[0 \infty]$ therefore before applying the GDQM we will convert the computational domain to $[0 \ 1]$. In order to achieve this objective, we have established the following transformations.

$$\left. \begin{aligned} \eta &= g(\xi) \\ f(\eta) &= f(g(\xi)) = F(\xi) \\ \theta(\eta) &= \theta(g(\xi)) = H(\xi) \end{aligned} \right\}. \quad (24)$$

Here

$$g(\xi) = \xi\eta_\infty, \quad (25)$$

and η_∞ is the value η where velocity and thermal boundary conditions meet asymptotically.

Using (24), we can express

$$\left. \begin{aligned} f^{(n)}(\eta) &= \frac{1}{\eta_\infty^n} F^{(n)}(\xi) \\ \theta^{(n)}(\eta) &= \frac{1}{\eta_\infty^n} H^{(n)}(\xi) \end{aligned} \right\}. \quad (26)$$

Here n in the superscript of $f(\eta)$, $F(\xi)$, $\theta(\eta)$ and $H(\xi)$ represents the n^{th} ordinary derivative w.r.t to the independent variable involved in the corresponding functions. Using (24) and (25) the nonlinear system (10)-(13) can be rewritten in the following way

$$L_F(F) + N_F(F, H) = 0, \quad (27)$$

$$L_H(H) + N_H(F, H) = 0, \quad (28)$$

$$F(0) = 1, \quad F'(1) \rightarrow 0, \quad F'(0) = \eta_\infty, \quad (29)$$

$$H(0) = 1, \quad H(1) \rightarrow 0. \quad (30)$$

Here $L_F(F)$, $N_F(F, H)$, $L_H(H)$ and $N_H(F, H)$ are defined as

$$L_F(F) = \frac{1}{\eta_\infty^3} F^{(3)}(\xi), \quad (31)$$

$$N_F(F, H) = \frac{1}{2\eta_\infty^2} F(\xi)F^{(2)}(\xi), \quad (32)$$

$$L_H(H) = \frac{N_R}{\eta_\infty^2} H^{(2)}(\xi), \quad (33)$$

$$N_H(F, H) = \left\{ \begin{aligned} &\frac{EcPrN_R}{\eta_\infty^2} F^{(2)}(\xi) + \frac{PrN_R F(\xi)H^{(1)}(\xi)}{2\eta_\infty} + \\ &\frac{4}{\eta_\infty^2} (\theta_r - 1)(H(\theta_r - 1) + 1)^2 \left(H^{(1)}(\xi) \right)^2 + \frac{4}{3\eta_\infty^2} H^{(2)}(\xi)(H(\theta_r - 1) + 1)^3 \end{aligned} \right\}. \quad (34)$$

The expression for Bejan number and entropy generation can be re-written as

$$Ns(\xi) = \frac{(\theta_r - 1)^2 (H^{(1)})^2}{\eta_\infty^2 (H(\theta_r - 1) + 1)^2} + \frac{Ec \Pr (F^{(2)})^2 (\theta_r - 1)}{\eta_\infty^4 H(\theta_r - 1) + 1} + \frac{4(H(\theta_r - 1) + 1)(H^{(1)})^2 (\theta_r - 1)^2}{3\eta_\infty^2 N_R}, \quad (35)$$

$$Be(\xi) = \frac{(3N_R + 4(H(\theta_r - 1) + 1)^3) \left(\frac{H^{(1)}}{\eta_\infty}\right)^2 (\theta_r - 1)}{3N_R(\theta_r - 1) \left(\frac{H^{(1)}}{\eta_\infty}\right)^2 + 3N_R Ec \Pr \left(\frac{F^{(2)}}{\eta_\infty^2}\right)^2 (H(\theta_r - 1) + 1) + 4(\theta_r - 1)(H(\theta_r - 1) + 1)^3 \left(\frac{H^{(1)}}{\eta_\infty}\right)^2}. \quad (36)$$

The Gauss-Lobatto grid points, which are well-suited for non-uniform spatial variable discretization, can be calculated using the formula presented below.

$$\xi_i = \frac{1}{2} \left(1 + \cos \left(\frac{(1-i)\pi}{N-1} \right) \right). \quad (37)$$

Here N denotes a total count of Gauss-Lobatto grid points. The following formulas yield the derivative of the functions F and H with respect to ξ at the grid points ξ_i

$$\frac{d^n F(\xi_i)}{d\xi^n} = \sum_{j=1}^N D_{ij}^{(n)} F(\xi_j) = \sum_{j=1}^N D_{ij}^{(n)} F_j, \quad 1 \leq i, j \leq N \quad (38)$$

$$\frac{d^n H(\xi_i)}{d\xi^n} = \sum_{j=1}^N D_{ij}^{(n)} H(\xi_j) = \sum_{j=1}^N D_{ij}^{(n)} H_j, \quad 1 \leq i, j \leq N. \quad (39)$$

As stated by Shu [31]

$$\left\{ \begin{array}{l} D_{ij}^{(1)} = \frac{\prod_{l=1, l \neq i}^N (\xi_i - \xi_l)}{(\xi_i - \xi_j) \prod_{l=1, l \neq j}^N (\xi_j - \xi_l)} \quad \text{for } i \neq j, \\ D_{ij}^{(1)} = - \sum_{j=1, j \neq i}^N D_{ij}^{(1)} \quad \text{for } i = j, \end{array} \right. \quad (40)$$

$$\left\{ \begin{array}{l} D_{ij}^{(n)} = n \left(D_{ii}^{(n-1)} D_{ij}^{(1)} - \frac{D_{ij}^{(n-1)}}{(\xi_i - \xi_j)} \right) \quad \text{for } i \neq j, \\ D_{ij}^{(n)} = - \sum_{j=1, j \neq i}^N D_{ij}^{(n)} \quad \text{for } i = j. \end{array} \right. \quad (41)$$

Here, $n \geq 2$ and $1 \leq i, j \leq N$.

By implementing the discretized form of the variables F , H , and their derivatives into the system (27–30), the resulting discretized system can be written as follows

$$S_{NL}(\xi_i) = \begin{cases} H(\xi_i) = 1, \text{ when } i = 1, \\ L_{H(i)}(\xi_i) + N_{H(i)}(H(\xi_i), G(\xi_i)) = 0, \text{ for } 2 \leq i \leq N - 1, \\ H(\xi_i) = 0, \text{ when } i = N, \\ F(\xi_i) = 0, \sum_{j=1}^N D_{ij}^{(1)} F_j - \eta_\infty = 0, \text{ when } i = 1, \\ L_{F(i)}(F(\xi_i)) + N_{F(i)}(F(\xi_i), H(\xi_i)) = 0, \text{ for } 3 \leq i \leq N - 1 \\ \sum_{j=1}^N D_{ij}^{(1)} F_j = 0, \text{ when } i = N. \end{cases} \quad (42)$$

$$L_{F(i)}(F_i) = \frac{1}{\eta_\infty^3} \sum_{j=1}^N D_{ij}^{(3)} F_j, \quad (43)$$

$$N_{F(i)}(F_i, H_i) = \frac{1}{2\eta_\infty^2} F(\xi_i) \sum_{j=1}^N D_{ij}^{(2)} F_j, \quad (44)$$

$$L_{H(i)}(H_i) = \frac{N_R}{\eta_\infty^2} \sum_{j=1}^N D_{ij}^{(2)} H_j, \quad (45)$$

$$N_{H(i)}(F_i, H_i) = \begin{cases} \frac{EcPrN_R}{\eta_\infty^2} \sum_{j=1}^N D_{ij}^{(2)} F_j + \frac{PrN_R F_i \sum_{j=1}^N D_{ij}^{(1)} H_j}{2\eta_\infty} + \\ \frac{4}{\eta_\infty^2} (\theta_r - 1)(H_i(\theta_r - 1) + 1)^2 \left(\sum_{j=1}^N D_{ij}^{(1)} H_j \right)^2 + \frac{4}{3\eta_\infty^2} (H_i(\theta_r - 1) + 1)^3 \sum_{j=1}^N D_{ij}^{(2)} H_j \end{cases} \quad (46)$$

$S_{NL}(\xi_i)$, which stands for an algebraic system of nonlinear equations, is the discretized and transformed form of the nonlinear system $S_{NL}(\xi)$. The Newton-Raphson method is used repeatedly to solve this discretized system. Further, [Figure 2](#) shows a brief description of the applied numerical technique. It is possible to create the relationships shown below in order to compute the discretized solution with respect to the variable η , velocity $f'(\eta)$, temperature $\theta(\eta)$, entropy generation $Ns(\eta)$ and $Be(\eta)$.

$$\frac{df(\eta_i)}{d\eta} = \frac{1}{\eta_\infty} \sum_{j=1}^N D_{ij}^{(1)} F(\chi_j), \quad (47)$$

$$\theta(\eta_i) = H(\xi_i), \quad (48)$$

$$Ns(\eta_i) = Ns(\xi_i), \quad (49)$$

where

$$\eta_i = \eta_\infty \left(1 + \cos \left(\frac{\pi(1-i)}{N-1} \right) \right). \quad (50)$$

5. Results and discussion

The purpose of this section is to examine the effects of different physical parameters on the variables of interest. To attain this objective, we have plotted [Figures \(3–6\)](#).

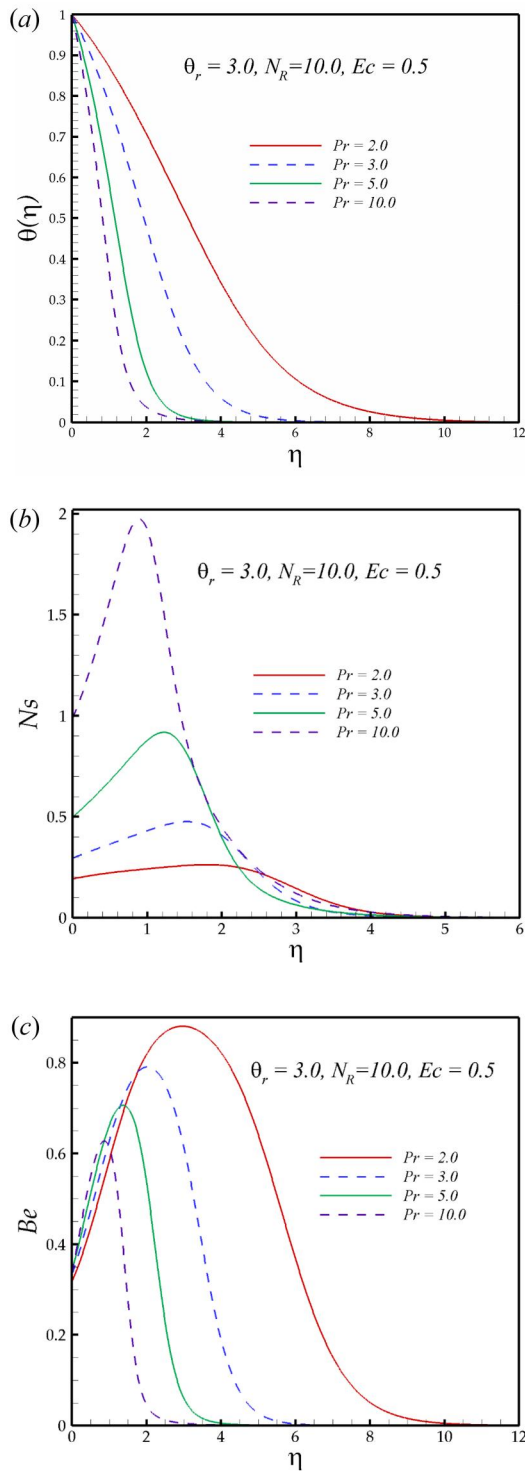


Figure 3. (a) Influence of Pr on $\theta(\eta)$. (b) Influence of Pr on Ns . (c) Influence of Pr on Be .

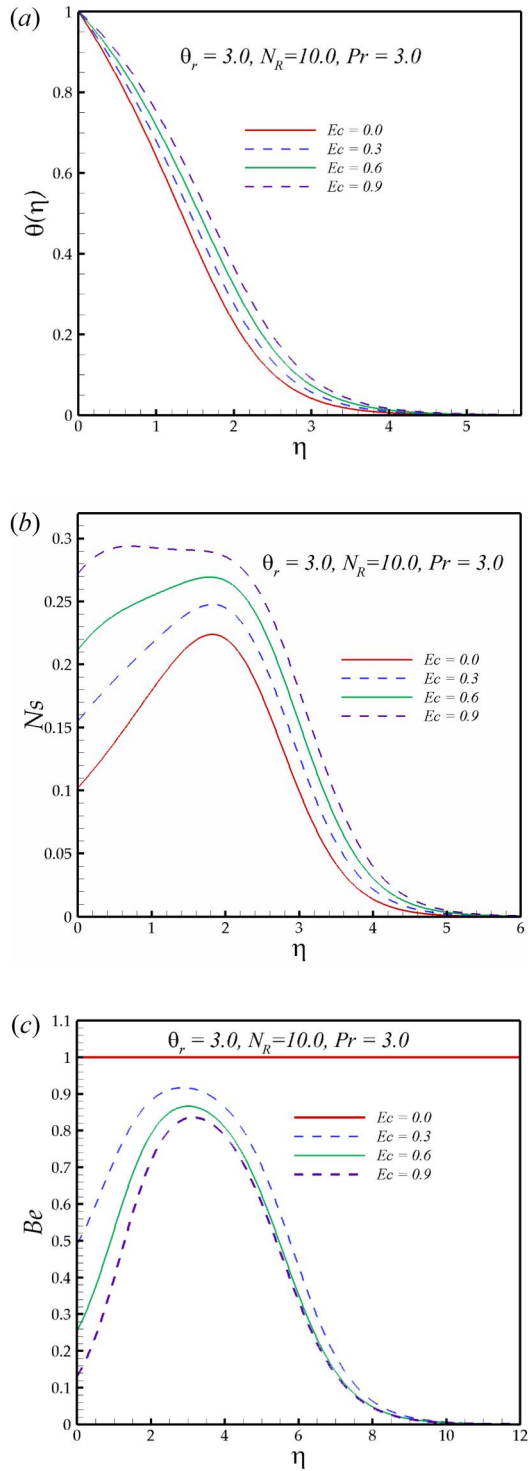


Figure 4. (a) Impact of Ec on $\theta(\eta)$. (b) Impact of Ec on N_s . (c) Influence of Ec on Be .

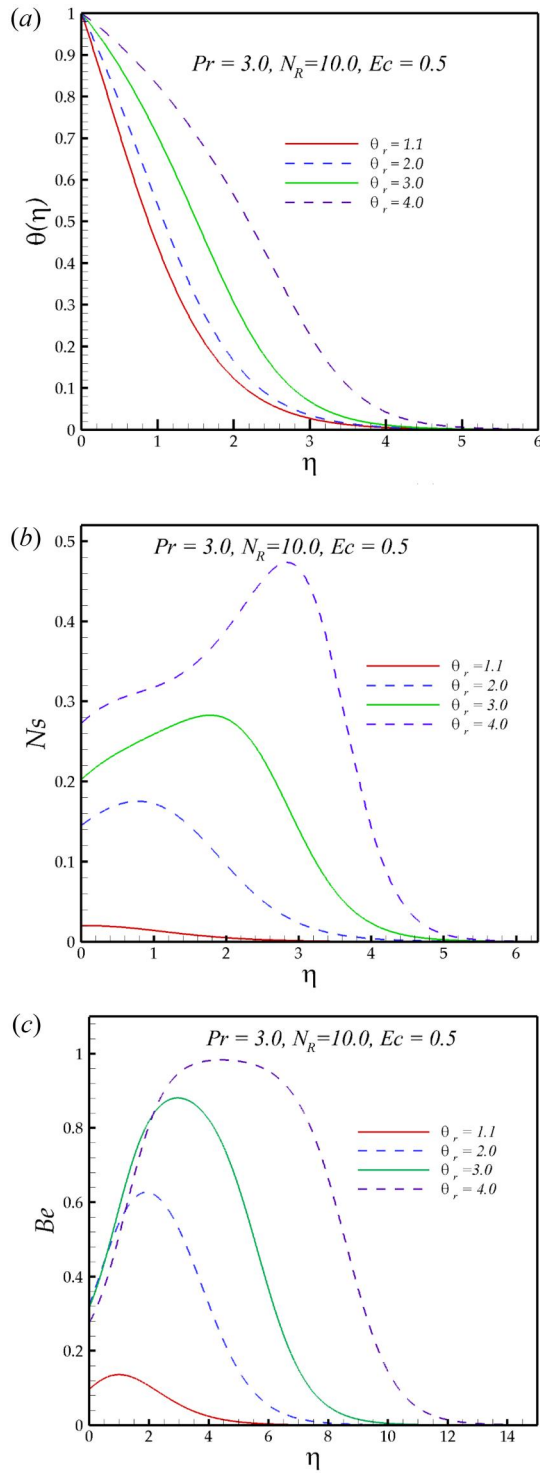


Figure 5. (a) Influence of θ_r on $\theta(\eta)$. (b) Influence of θ_r on Ns . (c) Influence of θ_r on Be .

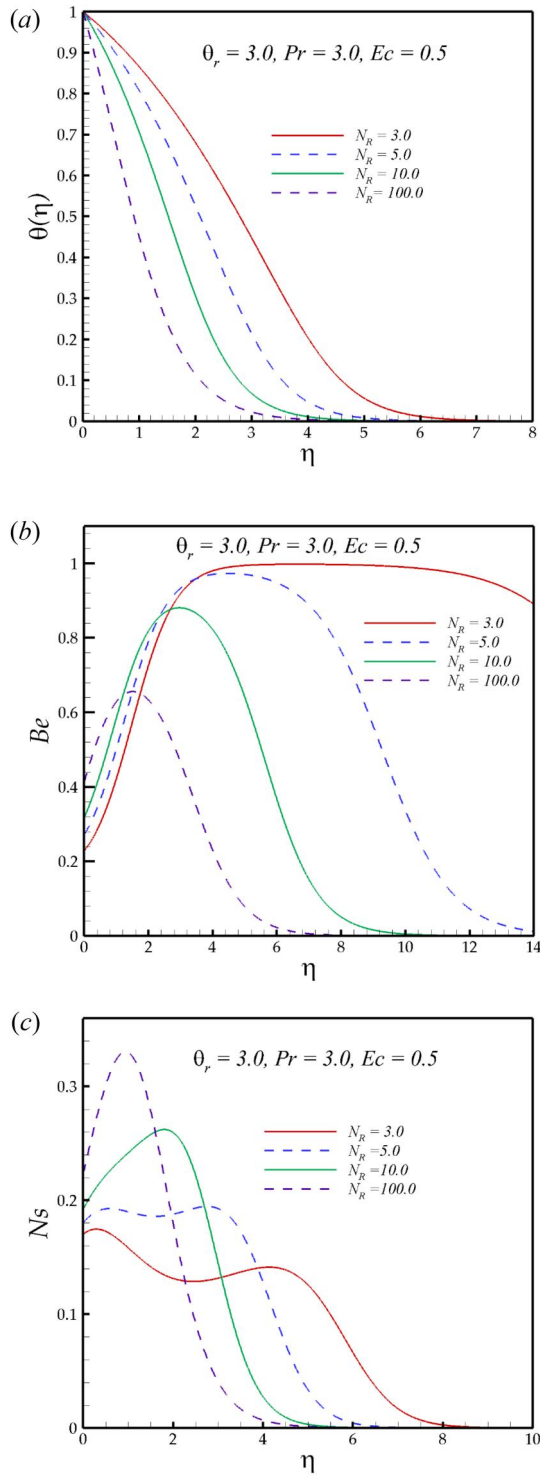


Figure 6. (a) Influence of N_R on $\theta(\eta)$. (b) Influence of N_R on Ns . (c) Influence of N_R on Be .

Table 1. Comparison with existing literature.

| η | $f(\eta)$ | | $f'(\eta)$ | | $-f''(\eta)$ | |
|--------|--------------|-----------------|--------------|-----------------|--------------|-----------------|
| | Cortell [13] | Present Results | Cortell [13] | Present Results | Cortell [13] | Present Results |
| 0.0 | 0.0 | 0.01 | 1.0 | 1.0 | 0.44374733 | 0.44374831 |
| 0.1 | 0.0977822 | 0.0977821 | 0.9556616 | 0.9556617 | 0.4426557 | 0.4426566 |
| 0.2 | 0.1911395 | 0.1911395 | 0.9115386 | 0.9115387 | 0.4394617 | 0.43946280 |
| 0.3 | 0.2801039 | 0.2801039 | 0.8678343 | 0.8678345 | 0.4343068 | 0.43430792 |
| 0.4 | 0.3647266 | 0.3647266 | 0.8247367 | 0.8247371 | 0.4273539 | 0.42735500 |
| 0.5 | 0.4450772 | 0.4450772 | 0.7824172 | 0.7824175 | 0.4187816 | 0.41878276 |
| 0.6 | 0.5212411 | 0.5212412 | 0.7410279 | 0.7410282 | 0.4087787 | 0.40878000 |
| 0.7 | 0.5933182 | 0.5933184 | 0.7007023 | 0.7007027 | 0.3975390 | 0.39754030 |
| 0.8 | 0.6614207 | 0.6614210 | 0.6615546 | 0.6615549 | 0.3852561 | 0.38525733 |
| 0.9 | 0.7256714 | 0.7256718 | 0.6236793 | 0.6236797 | 0.3721195 | 0.37212075 |
| 1.0 | 0.7862015 | 0.7862019 | 0.5871525 | 0.5871531 | 0.3583114 | 0.35831280 |
| 1.5 | 0.7862015 | 1.0380131 | 0.4262417 | 0.4262425 | 0.2847749 | 0.28477603 |
| 2.0 | 1.0380120 | 1.2185531 | 0.3017830 | 0.3017838 | 0.2145047 | 0.21450575 |
| 3.0 | 1.2185520 | 1.4327317 | 0.1440157 | 0.1440163 | 0.1098343 | 0.10983493 |
| 4.0 | 1.4327300 | 1.5330833 | 0.0662434 | 0.0662437 | 0.0521594 | 0.05215975 |
| 5.0 | 1.5330800 | 1.5788469 | 0.0299497 | 0.0299498 | 0.0239226 | 0.02392277 |
| 10 | 1.6154630 | 1.6154659 | 0.0005329 | 0.0005328 | 0.0004305 | 0.00043052 |
| 15 | 1.6161120 | 1.6161138 | 0.0000094 | 0.0000093 | 0.0000076 | 0.00000757 |
| 20 | 1.6161120 | 1.6161252 | 0.0000001 | 0.0000001 | 0.0000001 | 0.00000013 |

Table 2. Numerical values of $\frac{Nu_x}{(Re_x)^{1/2}} = -\theta'(0) \left(1 + \frac{4}{3N_R} (\theta_r)^3\right)$ against various values of Ec, Pr, N_R and θ_r .

| Ec | Pr | N_R | θ_r | $\frac{Nu_x}{(Re_x)^{1/2}} = -\theta'(0) \left(1 + \frac{4}{3N_R} (\theta_r)^3\right)$ |
|--------------------------------------|------|-------|------------|--|
| 0.2 | | | | 1.2059307 |
| 0.5 | 3.0 | 10.0 | 3.0 | 1.0097893 |
| 0.8 | | | | 0.8123688 |
| S_{ip} : Slope (Linear Regression) | | | | -0.655 |
| | 3.0 | | | 0.9441230 |
| 0.6 | 5.0 | 10.0 | 3.0 | 1.2275531 |
| | 6.8 | | | 1.4189249 |
| S_{ip} : Slope (Linear Regression) | | | | 0.125 |
| | | 3.0 | | 1.3623372 |
| 0.6 | 3.0 | 5.0 | 3.0 | 1.1714394 |
| | | 100.0 | | 0.5962210 |
| S_{ip} : Slope (Linear Regression) | | | | -0.007 |
| | | | 1.1 | 0.5852195 |
| 0.6 | 3.0 | 10.0 | 2.0 | 0.7127636 |
| | | | 4.0 | 1.2108934 |
| S_{ip} : Slope (Linear Regression) | | | | 0.221 |

As shown in Table 1, we compared the current findings with those found in the literature in order to validate our numerical solution. Strong agreement between the two was found in the comparison, supporting the accuracy of our computations. Table 2 depicts the effect of several physical parameters on the Nusselt number. The negative and positive slopes represent a drop and an increase in the Nusselt number values related to changes in these physical parameters, respectively. It has been noted that the Nusselt number declines as the Eckert number rises. Convective heat transmission is less effective than conductive heat transfer as the Eckert number rises, indicating a more energetic flow. The Nusselt number declines as a result of this. Table 2 shows that the Nusselt number grows as the Prandtl number increases. The fluid’s capacity to transfer heat through convection, as compared to conduction, decreases as the Prandtl number rises. The Nusselt number falls as a result of a weakening of convective heat transport within the boundary layer. The less effective convective heat transfer caused by, the shorter thermal boundary layer and decreased temperature gradient linked to higher

Prandtl numbers is the underlying physical cause. The Nusselt number reduces with N_R but the low value of S_p show a weak relation. The positive value of S_p indicates that Nusselt number rises with enhancing values of θ_r .

5.1. Impacts of Prandtl number

The Prandtl number, a non-dimensional parameter, establishes a connection between the viscosity and thermal conductivity of a fluid. It evaluates the interplay between the fluid's momentum transfer and thermal diffusion capabilities. Figure 3(a) in the research illustrates the influence of the Prandtl number on the temperature profile. The study revealed that an increase in the Prandtl number resulted in a gradual decrease in temperature within the boundary layer. Furthermore, the temperature approached zero asymptotically as the transverse distance increased. The observed reduction in temperature as a function of increasing Prandtl number can be related to the inverse correlation between the Prandtl number and the thermal diffusivity of the fluid. Physically, as the Prandtl number rises, it signifies a higher thermal diffusivity in relation to momentum diffusivity. To put it differently, heat is conveyed with greater efficiency in comparison to the transmission of momentum. Figure 3(b) illustrates the impact of the Prandtl number on the entropy generation number. The study revealed that the entropy observed at the surface of the plate exhibited a positive correlation with the Prandtl number. The entropy generation number increased in proximity to the plate at a fixed Pr value, followed by a subsequent decrease beyond a certain η value until reaching the boundary layer's edge. Additionally, it was observed that the impacts of irreversibility were more pronounced in the vicinity of the plate surface for fluids with high Prandtl number in contrast to those with low Prandtl number. Figure 3(c) depicts the impact of the Prandtl number on the Bejan number. The study revealed that, at a constant Pr value, the Bejan number exhibited an initial rise followed by a decline beyond a specific η value. Furthermore, the predominance of frictional effects in the generation of entropy was observed in comparison to the heat transfer effect in the proximity of the plate surface. With an increase in transverse distance (η), there was a corresponding increase in the proportion of heat transfer involved in entropy generation.

5.2. Impacts of Eckert number

The Eckert number establishes a connection between the kinetic energy and the enthalpy of a fluid. Physically, this parameter is used to explain the impact of self-heating within a fluid due to dissipation phenomena. The impact of Eckert number on the temperature profile is depicted in Figure 4(a). The rise in Ec leads to a corresponding increase in temperature due to heightened fluid friction among adjacent fluid layers, resulting in the conversion of kinetic energy into thermal energy. Furthermore, it can be observed that an increase in Ec results in a corresponding increase in the thickness of the thermal boundary layer. The Figure 4(b) illustrates the impact of Ec on the entropy generation number N_s . It is observed that N_s increases in proximity to the surface of the plate at a specific transversal distance ($\eta = 2.0$) but subsequently decreases and ultimately ceases within the primary flow region. The decrease in the Bejan number is observed in Figure 4(c) as the value of Ec increases. The production of entropy when the potential energy is at zero is solely attributed to the transfer of heat. For non-zero value of Ec , the Bejan number exhibits an initial increase until reaching a fixed value, followed by a continuous decrease and eventual disappearance within the primary flow region.

5.3. Impacts of heating parameter

Heating parameter is the ration of wall temperature and ambient temperature. In present problem, it's values should be greater than one because the wall temperature is greater than the ambient temperature. Physically, increasing values of heating parameter shows the increasing

temperature difference between wall and ambient fluid. Figure 5(a) displays the effect of the heating parameter θ_r on the temperature profile. An elevation in the parameter θ_r induces a wider temperature distribution, plausibly attributable to an escalation in the operational temperature ΔT . This, in turn, leads to a greater fraction of the fluid within the boundary layer attaining high temperature, characterized by high thermal diffusivity $\left(\alpha + \frac{16\sigma_{SB}}{3\rho C_p a_R} T^3\right)$ and a thick thermal boundary layer. The impact of θ_r on the entropy generation number N_s is illustrated in Figure 5(b). The results indicate that the entropy exhibits an upward trend with θ_r in the vicinity of the boundary and its immediate surroundings. However, it experiences a decline after attaining the highest point. Furthermore, it has been demonstrated that the existence of nonlinear Rosseland thermal radiation results in increased entropy generation in comparison to the linear Rosseland thermal approximation. The findings presented in Figure 5(c) indicate a positive correlation between the Bejan number Be and the heating parameter. The role of fluid friction in generating entropy is significant both at the boundary and in the surrounding region. As the temperature ratio θ_r increases, the contribution of heat transfer to entropy production becomes increasingly important.

5.4. Impacts of radiation parameter

The radiation parameter N_R is used to specify the proportionate impact of conductive heat transfer in comparison to thermal radiation transfer. The impact of radiation parameter N_R on the temperature profile θ is depicted in Figure 6(a). It can be observed that an increase in N_R results in a reduction of fluid temperature and a thinner temperature profile. For a given value of k and a_R , a rise in $N_R = \frac{ka_R}{4\sigma_{sb}T_\infty^3}$ results in a drop in ambient temperature T_∞ , implying that a major portion of the fluid inside the boundary layer has a low temperature and a low thermal diffusivity $\left(\alpha + \frac{16\sigma_{SB}}{3\rho C_p a_R} T^3\right)$ with a thin thermal boundary layer. As an alternative, Equation (7) states that a drop in a_R causes a rise in the term q_r , which reduces the amount of heat that is transferred to the fluid *via* radiation and thus lowers the fluid's temperature. The findings depicted in Figure 6(b) indicate that the entropy generation number experiences an increase in proximity to the surface as well as in its immediate vicinity, while it undergoes a decrease in the region that is situated at a distance from the boundary, as the value of N_R is raised. The evidence suggests that the maximum entropy is located within the boundary layer rather than at its boundary. Moreover, it has been observed that the Bejan number, denoted as Be , exhibits an increasing trend in the vicinity of the surface and in its proximity as the values of N_R increase. Conversely, it shows a decreasing trend away from the boundary, indicating that the impact of fluid friction becomes more pronounced in the vicinity of the boundary layer's edge.

6. Concluding remarks

The present investigation examined the Sakiadis flow under the influence of nonlinear Rosseland thermal radiation and energy dissipation, with a focus on entropy generation. Some of the significant findings of the study are

- A self-similar solution can be obtained in the presence of viscous dissipation.
- The reduction of entropy generation can be achieved through the minimization of the difference in temperature between the ambient temperature and the wall.
- As the parameters Pr and N_R are augmented, the entropy exhibits an increment in proximity to the boundary, whereas it experiences a decrement in the area that is distant from the surface.
- The boundary does not contribute significantly to the generation of entropy. Rather, the highest number of entropy generation is observed within the boundary layer.

- The dominant factor cause entropy generation at the boundary is fluid friction, as compared to heat transfer.
- The quality of energy is enhanced through the reduction of the heating parameter.
- The widening of the temperature profile is observed with an increase in both Ec and θ_r .

Future work

The mathematical model exhibits local non-similarity when subjected to a constant magnetic field and is a topic for future investigation. Despite common practice among many authors to consider it as self-similar, addressing the local non-similarity as self-similar leads to imprecise outcomes. Moreover, the examination of electrical conductivity as a function of temperature is a topic that requires further investigation and may generates significant interest.

Disclosure statement

No potential conflict of interest was reported by the author(s).

Funding

This research is supported by Provincial Department of Education Philosophy and Social Science. Research Project (No.: 22Q216) 2021 School-Level Scientific Research Project (No. XJ2021003401).

ORCID

Muhammad Idrees Afridi  <http://orcid.org/0000-0002-8818-5980>

Ali J. Chamkha  <http://orcid.org/0000-0002-8335-3121>

References

- [1] J. W. Smith, "Effect of gas radiation in the boundary layer on aerodynamic heat transfer," *J. Aeronaut. Sci.*, vol. 20, no. 8, pp. 579–580, Aug. 1953. DOI: [10.2514/8.2740](https://doi.org/10.2514/8.2740).
- [2] C. Perdikis and A. Raptis, "Heat transfer of a micropolar fluid by the presence of radiation," *Heat Mass Transf.*, vol. 31, no. 6, pp. 381–382, 1996. DOI: [10.1007/BF02172582](https://doi.org/10.1007/BF02172582).
- [3] K.-L. Hsiao, "Energy conversion conjugate conduction–convection and radiation over non-linearly extrusion stretching sheet with physical multimedia effects," *Energy*, vol. 59, pp. 494–502, 2013. DOI: [10.1016/j.energy.2013.06.041](https://doi.org/10.1016/j.energy.2013.06.041).
- [4] A. J. Chamkha, H. S. Takhar and V. M. Soundalgekar, "Radiation effects on free convection flow past a semi-infinite vertical plate with mass transfer," *Chem. Eng. J.*, vol. 84, no. 3, pp. 335–342, 2001. DOI: [10.1016/S1385-8947\(00\)00378-8](https://doi.org/10.1016/S1385-8947(00)00378-8).
- [5] K. Vajravelu, G. Sarojamma, K. Sreelakshmi and C. Kalyani, "Dual solutions of an unsteady flow, heat and mass transfer of an electrically conducting fluid over a shrinking sheet in the presence of radiation and viscous dissipation," *Int. J. Mech. Sci.*, vol. 130, pp. 119–132, 2017. DOI: [10.1016/j.ijmecsci.2017.05.040](https://doi.org/10.1016/j.ijmecsci.2017.05.040).
- [6] O. D. Makinde and A. Ogulu, "The effect of thermal radiation on the heat and mass transfer flow of a variable viscosity fluid past a vertical porous plate permeated by a transverse magnetic field," *Chem. Eng. Commun.*, vol. 195, no. 12, pp. 1575–1584, Aug. 2008. DOI: [10.1080/00986440802115549](https://doi.org/10.1080/00986440802115549).
- [7] K.-L. Hsiao, "To promote radiation electrical MHD activation energy thermal extrusion manufacturing system efficiency by using Carreau-Nanofluid with parameters control method," *Energy*, vol. 130, pp. 486–499, 2017. DOI: [10.1016/j.energy.2017.05.004](https://doi.org/10.1016/j.energy.2017.05.004).
- [8] E. Magyari and A. Pantokratoras, "Note on the effect of thermal radiation in the linearized Rosseland approximation on the heat transfer characteristics of various boundary layer flows," *Int. Commun. Heat Mass Transf.*, vol. 38, no. 5, pp. 554–556, 2011. DOI: [10.1016/j.icheatmasstransfer.2011.03.006](https://doi.org/10.1016/j.icheatmasstransfer.2011.03.006).
- [9] A. Pantokratoras and T. Fang, "Sakiadis flow with nonlinear Rosseland thermal radiation," *Phys. Scr.*, vol. 87, no. 1, pp. 015703, 2013. DOI: [10.1088/0031-8949/87/01/015703](https://doi.org/10.1088/0031-8949/87/01/015703).

- [10] A. Pantokratoras and T. Fang, “Blasius flow with non-linear Rosseland thermal radiation,” *Meccanica*, vol. 49, no. 6, pp. 1539–1545, 2014. DOI: [10.1007/s11012-014-9911-3](https://doi.org/10.1007/s11012-014-9911-3).
- [11] B. C. Sakiadis, “Boundary-layer behavior on continuous solid surfaces: i. Boundary-layer equations for two-dimensional and axisymmetric flow,” *AICHE J.*, vol. 7, no. 1, pp. 26–28, 1961. DOI: [10.1002/aic.690070108](https://doi.org/10.1002/aic.690070108).
- [12] F. K. Tsou, E. M. Sparrow and R. J. Goldstein, “Flow and heat transfer in the boundary layer on a continuous moving surface,” *Int. J. Heat Mass Transf.*, vol. 10, no. 2, pp. 219–235, 1967. DOI: [10.1016/0017-9310\(67\)90100-7](https://doi.org/10.1016/0017-9310(67)90100-7).
- [13] R. Cortell, “A numerical tackling on Sakiadis flow with thermal radiation,” *Chinese Phys. Lett.*, vol. 25, no. 4, pp. 1340–1342, 2008. DOI: [10.1088/0256-307X/25/4/048](https://doi.org/10.1088/0256-307X/25/4/048).
- [14] H. S. Takhar, S. Nitu and I. Pop, “Boundary layer flow due to a moving plate: variable fluid properties,” *Acta Mech.*, vol. 90, no. 1–4, pp. 37–42, 1991. DOI: [10.1007/BF01177397](https://doi.org/10.1007/BF01177397).
- [15] V. G. Fox, L. E. Erickson and L. T. Fan, “Methods for solving the boundary layer equations for moving continuous flat surfaces with suction and injection,” *AICHE J.*, vol. 14, no. 5, pp. 726–736, DOI: [10.1002/aic.690140510](https://doi.org/10.1002/aic.690140510).
- [16] N. Afzal, A. Badaruddin and A. A. Elgarvi, “Momentum and heat transport on a continuous flat surface moving in a parallel stream,” *Int. J. Heat Mass Transf.*, vol. 36, no. 13, pp. 3399–3403, 1993. (93)90022-X. DOI: [10.1016/0017-9310](https://doi.org/10.1016/0017-9310).
- [17] A. Ishak, “Radiation effects on the flow and heat transfer over a moving plate in a parallel stream,” *Chinese Phys. Lett.*, vol. 26, no. 3, pp. 034701, 2009. DOI: [10.1088/0256-307X/26/3/034701](https://doi.org/10.1088/0256-307X/26/3/034701).
- [18] O. D. Makinde, “Analysis of Sakiadis flow of nanofluids with viscous dissipation and Newtonian heating,” *Appl. Math. Mech.-Engl. Ed.*, vol. 33, no. 12, pp. 1545–1554, Dec. 2012. DOI: [10.1007/s10483-012-1642-8](https://doi.org/10.1007/s10483-012-1642-8).
- [19] A. Pantokratoras, “The Blasius and Sakiadis flow along a Riga-plate,” *PCFD*, vol. 11, no. 5, pp. 329–333, Jan. 2011. DOI: [10.1504/PCFD.2011.042184](https://doi.org/10.1504/PCFD.2011.042184).
- [20] M. I. Afridi, M. Qasim and I. Khan, “Entropy generation minimization in MHD boundary layer flow over a slendering stretching sheet in the presence of frictional and joule heating,” *J. Korean Phys. Soc.*, vol. 73, no. 9, pp. 1303–1309, Nov. 2018. DOI: [10.3938/jkps.73.1303](https://doi.org/10.3938/jkps.73.1303).
- [21] M. I. Afridi and M. Qasim, “Second law analysis of Blasius flow with nonlinear Rosseland thermal radiation in the presence of viscous dissipation,” *Propuls. Power Res.*, vol. 8, no. 3, pp. 234–242, 2019. DOI: [10.1016/j.jprr.2018.06.001](https://doi.org/10.1016/j.jprr.2018.06.001).
- [22] M. I. Afridi, M. Qasim, N. A. Khan and O. D. Makinde, “Minimization of entropy generation in MHD mixed convection flow with energy dissipation and joule heating: utilization of Sparrow-Quack-Boerner local non-similarity method,” *DDF*, vol. 387, pp. 63–77, 2018. DOI: [10.4028/www.scientific.net/DDF.387.63](https://doi.org/10.4028/www.scientific.net/DDF.387.63).
- [23] A. S. Butt, K. Maqbool, S. M. Imran and B. Ahmad, “Entropy generation effects in MHD Casson nanofluid past a permeable stretching surface,” *IJEX*, vol. 31, no. 2, pp. 150, 2020. DOI: [10.1504/IJEX.2020.105481](https://doi.org/10.1504/IJEX.2020.105481).
- [24] M. Qasim and M. I. Afridi, “Effects of energy dissipation and variable thermal conductivity on entropy generation rate in mixed convection flow,” *J. Therm. Sci. Eng. Appl.*, vol. 10, no. 4, Aug. 2018. DOI: [10.1115/1.4038703](https://doi.org/10.1115/1.4038703).
- [25] M. I. Afridi and M. Qasim, “Comparative study and entropy generation analysis of Cu–H₂O and Ag–H₂O nanofluids flow over a slendering stretching surface,” *J. Nanofluids*, vol. 7, no. 4, pp. 783–790, Aug. 2018. DOI: [10.1166/jon.2018.1488](https://doi.org/10.1166/jon.2018.1488).
- [26] S. Haider, A. S. Butt, S. M. Imran and A. Ali, “Study of entropy generation impacts on magneto-hydrodynamic flow and heat transmission over a contracting surface,” *SN Appl. Sci.*, vol. 1, no. 7, pp. 796, Jul. 2019. DOI: [10.1007/s42452-019-0828-2](https://doi.org/10.1007/s42452-019-0828-2).
- [27] M. I. Afridi, Z.-M. Chen, M. Qasim and O. D. Makinde, “Computational analysis of entropy generation minimization and heat transfer enhancement in magnetohydrodynamic oscillatory flow of ferrofluids,” *J. Magn. Magn. Mater.*, vol. 594, pp. 171848, Mar. 2024. DOI: [10.1016/j.jmmm.2024.171848](https://doi.org/10.1016/j.jmmm.2024.171848).
- [28] A. Aziz and W. A. Khan, “Minimum entropy generation design of a convectively heated pin fin with tip heat loss,” *IJEX*, vol. 10, no. 1, pp. 44–60, Jan. 2012. DOI: [10.1504/IJEX.2012.045060](https://doi.org/10.1504/IJEX.2012.045060).
- [29] M. I. Afridi, M. Qasim and S. Shafie, “Entropy generation in hydromagnetic boundary flow under the effects of frictional and Joule heating: exact solutions,” *Eur. Phys. J. Plus*, vol. 132, no. 9, pp. 404, Sep. 2017. DOI: [10.1140/epjp/i2017-11704-5](https://doi.org/10.1140/epjp/i2017-11704-5).
- [30] W. A. Khan and R. S. R. Gorla, “Second law analysis for free convection in non-newtonian fluids over a horizontal plate embedded in a porous medium: prescribed surface temperature,” *J. Heat Transfer.*, vol. 133, no. 5, pp. 511 – 518, Feb. 2011. DOI: [10.1115/1.4003045](https://doi.org/10.1115/1.4003045).
- [31] O. D. Makinde, W. A. Khan and A. Aziz, “On inherent irreversibility in Sakiadis flow of nanofluids,” *IJEX*, vol. 13, no. 2, pp. 159–174, Jan. 2013. DOI: [10.1504/IJEX.2013.056131](https://doi.org/10.1504/IJEX.2013.056131).